Elsevier Editorial System(tm) for Journal of Solid State Chemistry

Manuscript Draft

Manuscript Number: JSSC-15-1071R1

Title: Structure and Magnetic Properties of Flux Grown Single Crystals of Co3-xFexSn2S2 Shandites.

Article Type: Research Paper

Keywords: Sulfides; Tow dimensional structures; Crystal growth, X-ray diffraction; Magnetic materials.

Corresponding Author: Mr. Mohamed A. Kassem, Ph.D.

Corresponding Author's Institution: Kyoto University

First Author: Mohamed A. Kassem, Ph.D.

Order of Authors: Mohamed A. Kassem, Ph.D.; Yoshikazu Tabata, Prof. Dr.; Takeshi Waki, Dr.; Hiroyuki Nakamura, Prof. Dr.

Abstract: We report a successful single crystal growth of the shandite-type half metallic ferromagnet Co3Sn2S2, and its Fe-substituted compounds, Co3□xFexSn2S2, by employing the flux method. Although Fe3Sn2S2 is unstable phase, we found that using the self Sn flux enables us to obtain single phase crystals up to x = 0.53. The chemical composition of the grown plate-shaped single crystals was examined using wavelength-dispersive X-ray spectroscopy. The shandite structure with R-3m symmetry was confirmed by powder X-ray diffraction and the crystal structure parameters were refined using the Rietveld method. Magnetization measurements show suppression of the ferromagnetic order upon Fe-substitution , as well as in other substituted systems such as In- and Ni-substituted Co3Sn2S2. The almost identical magnetic phase diagrams of the Fe- and In-substituted compounds indicate that the electron number is dominantly significant to the magnetism in the Co-based shandite.

Structure and Magnetic Properties of Flux Grown Single Crystals of $Co_{3-x}Fe_xSn_2S_2$ Shandites.

Mohamed A. Kassem[*,†] *, Yoshikazu Tabata, Takeshi Waki, Hiroyuki Nakamura.*

Department of Materials Science and Engineering, Kyoto University, Kyoto 606-8501, Japan.

ABSTRACT:

We report a successful single crystal growth of the shandite-type half metallic ferromagnet $Co_3Sn_2S_2$, and its Fe-substituted compounds, $Co_{3-x}Fe_xSn_2S_2$, by employing the flux method. Although $Fe_3Sn_2S_2$ is unstable phase, we found that using the self Sn flux enables us to obtain single phase crystals up to x = 0.53. The chemical composition of the grown plate-shaped single crystals was examined using wavelength-dispersive X-ray spectroscopy. The shandite structure with $R\bar{3}m$ symmetry was confirmed by powder X-ray diffraction and the crystal structure parameters were refined using the Rietveld method. Magnetization measurements show suppression of the ferromagnetic order upon Fe-substitution , as well as in other substituted systems such as In- and Ni-substituted $Co_3Sn_2S_2$. The almost identical magnetic phase diagrams of the Fe- and In-substituted compounds indicate that the electron number is dominantly significant to the magnetism in the Co-based shandite.

Key Words:

Sulfides; Tow dimensional structures; Crystal growth, X-ray diffraction; Magnetic materials.

1. Introduction

A need is growing to synthesis single crystals of transition metal-sulfur binaries and ternaries due to their functional properties that make them promising candidates for applications including photovolatics[1,2], thermoelectrics[3,4] and magnetic sensors[5,6]. Among of them, the ternary compounds with the general formula $T_3M_2X_2$ (with T = Ni, Co, Rh or Pd; M = In, Sn, Pb, Tl or Bi; and X = S or Se) crystallizing in the parkerite (M = Bi)[7] or shandite ($M \neq$ Bi)[8] structure have been investigated extensively in recent decades[9–17]. Fascinating electronic properties were proposed by the electronic band calculations and novel phenomena were discovered experimentally, for instance the superconductivity in the parkerite $Ni_3Bi_2S_2$[18] and the half-metallic ferromagnetism in the shandite $Co_3Sn_2S_2$[12,13]. As the only shandite compounds showing magnetic ordering, $Co_3Sn_2S_2$ and its solid solutions have a particular interest in recent studies of shandites[12,13,19–23]. Figure 1, illustrated by the VESTA software[24], shows the shandite type crystal structure of $Co_3Sn_2S_2$ which belongs to the trigonal space group $R\bar{3}m$. The shandite-type crystal can be considered to consist of metallic layers stacked in ABC fashion along c-direction in a hexagonal notation. As shown in Fig. 1a, both Co and S atoms occupy the unique sites 9*e* (1/2,0,0) and 6*c* (0,0,z), respectively, while Sn atoms occupy two different sites; a half of Sn atoms occupies the inter-layer 3*b* (0,0,1/2) site (Sn1-site) and the other half occupies the intra-layer 3*a* (0,0,0) site (Sn2-site). The layers are arranged in the kagomé network of corner-sharing triangles of Co atoms and triangular lattice of the Sn atoms on 3*a*-site (see Fig. 1b). Each Co triangle is alternately caped above and below by an S atom. The Co-Sn2 layers are connected via the interlayer Sn1 atoms. The Co atom is octahedrally surrounded by two Sn1, two Sn2, and two S atoms with the trigonal symmetry.

$Co_3Sn_2S_2$ is a ferromagnetic metal of Curie temperature of 174 K and spontaneous magnetic moment of $\sim 0.3\ \mu_B$/Co in the easy axis[23,25]. The half metallic ferromagnetism of $Co_3Sn_2S_2$, which is a key ingredient for high performance of spintronics devices, was proposed by the band calculation[12,23] and experimentally confirmed by the photoemission study[26]. Moreover, promising thermoelectric properties[20,21] and magnetic quantum phase transitions[13,27] were expected in its solid solutions. For

example, it was found that the magnetism of $Co_3Sn_2S_2$ is very sensitive to the chemical substitution and is suppressed upon substitutions of In for Sn[13,27], Se for S[28,29] and Ni or Fe for Co[30,31]. Unfortunately, the above-mentioned solid solutions, except for the parent compound $Co_3Sn_2S_2$[23], were investigated using polycrystalline samples and no experiment using single crystals solid solutions had been reported. Recently, we firstly succeeded to grow single crystals of the In-substitution compounds for full In-concentration region and reported their crystal structure parameters and magnetic properties briefly[25]. The success of growing single crystals should allow to investigate the interesting electronic and magnetic properties of the In-substituted $Co_3Sn_2S_2$ in more details.

Although the Fe-based shandite $Fe_3Sn_2S_2$ is unstable, the first experimental trial to synthesis polycrystalline samples of the solid solution $Co_{3-x}Fe_xSn_2S_2$ is recently reported[31]. They found that the solubility limit of $Co_{3-x}Fe_xSn_2S_2$ is $x \sim 0.6$ at ambient pressure and can be extended to $x \sim 1$ by the high temperature and pressure heat treatment. Magnetization measurements using the obtained polycrystalline samples showed that the ferromagnetic order in this system is suppressed upon Fe-substitution and the critical composition of the non-magnetic to magnetic transition was estimated by extrapolating the obtained magnetic phase diagram to be $x = 1.5$. Moreover, a semiconducting gap opening was predicted by the electronic band structure calculations for $x = 1.0$[31], which suggests high thermoelectric properties as observed in the In-substituted system[20]. The success of growing single crystals of $Co_{3-x}Fe_xSn_2S_2$ allows us to investigate its intriguing properties in more details, especially the anisotropic properties implied by the layered crystal structure of this system. Moreover we expect interesting magnetic effects of the spin-frustrated Kagomé Co networks which can emerge in this solid solution.

In this article, we report on successful single crystal growth of $Co_{3-x}Fe_xSn_2S_2$ solid solution. We obtained the single crystals of $Co_{3-x}Fe_xSn_2S_2$ up to $x = 0.53$ out of Sn flux. Optimal conditions to obtain large single crystals are discussed. Results of characterizing the grown crystals by means of wavelength-dispersive X-ray spectroscopy (WDX), Laue X-ray photography, powder X-ray diffraction (PXRD) and

magnetization measurements are presented. The structural effects of Fe-substitution are followed by the Rietveld refinement using PXRD experimental data.

2. Experimental Details

Single crystals of $Co_{3-x}Fe_xSn_2S_2$ ($0 \leq x \leq 0.53$) were grown by a flux method[32–36]. Synthesis of sulfide crystals out of a solid solution is challenging due to the low boiling point and polymeric nature of S. However many sulfur bearing single crystals have been grown out of binary sulfur-metal solutions[37]. Similarly to the growth of $Co_3Sn_2S_2$ single crystals[25], we used Sn as a self flux to grow $Co_{3-x}Fe_xSn_2S_2$. The appropriate ratio of constituent elements and the temperature profile of crystal growth were mainly chosen following ref. 37. Lumps of Co (99.9 % HIGH PURITY CHEMICALS) and Fe (99.95 % Alfa Aesar), Grains of Sn (99.999 % HIGH PURITY CHEMICALS) and grinded crystals of S (99.999 % nacalai tesque) were mixed in an initial mixture of molar ratios (Co + Fe): S: Sn = 8: 6: 86. The constituent was placed in a 5 mL Al_2O_3 growth crucible that was covered by another upside-down crucible filled with quartz wool. Both were sealed in an evacuated quartz ampoule, which was put in an electric furnace. After heated to 400 °C over 2 hours and held for extra 2 hours, the mixture was heated up to 1050 °C over 6 hours and kept for 6 hours to wait for the constituent melts homogeneously. The melt was cooled slowly to 700 °C over 70 hours. At 700 °C the ampoule was removed from the electric furnace and the flux was removed via rapid decanting and subsequent spinning in a centrifuge. Pb flux with grains of Pb (99.99 % RARE METALLIC CO., LTD.), which was found to be available for growing single crystals of $Co_3Sn_{2-y}In_yS_2$[25], was also employed in an initial composition of (Co + Fe): S: Sn: Pb = 6: 6: 36: 52 in a trial to extend the solubility of $Co_{3-x}Fe_xSn_2S_2$.

The chemical compositions were investigated by WDX to stand on the actual Fe content in the grown crystals. The grown crystals were characterized by PXRD at room temperature using an X-ray diffractometer (X'Pert Pro, PANalytical) with Cu $K_{\alpha 1}$ radiation monochromated by a Ge (111)-Johansson-type monochromator. The crystal structure parameters were refined from the PXRD data by the Rietveld method using the TOPAS software Version 5 (from Bruker AXS)[38]. The crystals were

oriented using a Laue X-ray camera. Magnetization measurements using a SQUID magnetometer (MPMS, Quantum Design) installed in the Research Center for Low Temperature and Materials Science, Kyoto University, were performed in a temperature range of 2 – 350 K and magnetic field up to 7 T.

3. Results and Discussions.

3.1. Crystal growth and chemical composition

Single crystals of the shandite-phase solid solution $Co_{3-x}Fe_xSn_2S_2$ were successfully grown out of Sn self flux with the starting Fe concentration up to $x_{nom} = 0.7$ in the molten. We found that single crystals of the shandite-phase are not grown with higher starting Fe concentrations. Instead, other phases such as SnS sheets, CoSn rods, FeS and $CoSn_2$ were found to be synthesized. It is consistent with a recent work to synthesis polycrystalline $Co_{3-x}Fe_xSn_2S_2$, where large amounts of by-products were found for $x_{nom} > 0.6$.

Fig. 2a shows images of grown single crystals of $Co_{3-x}Fe_xSn_2S_2$ out of Sn flux on a mm scale. The grown single crystals have a hexagonal sheet shape, reflecting the crystal structure. Sn flux is found to remain on the surface of the grown single crystals. To use the grown crystals for further investigations of physical properties of $Co_{3-x}Fe_xSn_2S_2$ shandites, mechanical polishing is required to remove the remaining flux on the surface. A back reflection Laue image taken from the large flat plane of a sheet shaped crystal is shown in Fig. 2b. It accords the calculated Laue pattern of the (001) plane under the $R\bar{3}m$ symmetry shown in Fig. 2c, indicating the large flat plane of the grown single crystal is the *c*-plane of the hexagonal crystal. The clear spots in the Laue image indicate high crystalline quality of the grown crystals.

Chemical compositions of the grown crystals measured by WDX are listed in Table 1. We confirmed the homogeneous compositions of the grown crystals by measuring the composition for each crystal at several locations on the surface. The listed compositions were obtained by averaging the WDX data for each crystal and were normalized by (Co + Fe)-concentration to 3. We should note that the measured Sn

and S concentrations in the solid solution are of 2.00 ± 0.06 and 1.90 ± 0.09, respectively, indicating stoichiometry of the grown single crystals. The actual Fe-concentration x is higher than the nominal x_{nom} for the low Fe-concentration crystals, whereas, x is saturated at about 0.5 for $x_{nom} > 0.5$. The maximum Fe concentration in the grown $Co_{3-x}Fe_xSn_2S_2$ crystals out of Sn self flux is $x = 0.53$. It is quantitatively consistent with the solubility limit of $x \sim 0.6$ in the polycrystalline sample at ambient pressure. By using Pb flux, the shandite-phase crystals were grown with the starting Fe concentration up to $x_{nom} = 1$, however, the actual Fe-concentration was found to be largely reduced as shown in Table 1.

3.2. Powder X-ray diffraction and crystal structure analysis

The crystal structure effects of the Fe-substituted $Co_{3-x}Fe_xSn_2S_2$ system is investigated by PXRD. The observed diffraction patterns are fitted using the structure parameters of the $Co_3Sn_2S_2$ shandite structure of $R\bar{3}m$ symmetry. The observed and calculated PXRD patterns of $Co_{3-x}Fe_xSn_2S_2$ at room temperature with representative Fe concentrations are shown in Fig. 3. The powder samples used for PXRD were prepared by crushing parts of the single crystals. PXRD patterns exhibit the shandite-phase as the main phase of the obtained crystals for all Fe concentrations. Relative small traces of the used flux as well as by-products such as $CoSn_2$, CoSn and/or SnS emerge in the PXRD patterns. To confirm that the remaining flux and by-products in the growth process exist only on the crystals surface, we performed PXRD for well-polished pieces of $Co_3Sn_2S_2$ single crystals. As shown in the inset of Fig. 3, the patterns of Sn and $CoSn_2$ emerged in the PXRD patterns used in the main figure are absent in that of the well-polished crystals. Thus, further accurate experiments, for instance the magnetization measurements described later, have been and will be performed using the well-polished crystals, whereas, the PXRD data of the crystals polished incompletely, shown in the main figure of Fig. 3, were used for the Rietveld analysis to obtain precise data sufficient for structure parameters refinement using the limited size crystals.

The lattice parameters and atomic position parameter of the S-site, z, refined by the Rietveld method are listed in Table 2, as well as lengths of T (Co/Fe) related bonds for all Fe concentrations. In the

analysis, we considered the extrinsic phases of the by-products mentioned above. The Co/Fe occupancies were confined based on the WDX results. The best fitting results are shown by red solid lines in Fig. 3. The low reliability *R*-factors and goodness-fit-indicator *S* indicate the satisfactory refinement for each Fe-concentration sample..

Fig. 4 shows the refined lattice parameters, *a* and *c*, plotted against Fe concentration *x*. The unit cell volume, *V*, as well as the *c* to *a* ratio against *x* are shown in the inset. The error bars of both *V* and *c*/*a* are in the range of the representative symbols. Whereas *a* decreases upon Fe-substitution, *c* and *V* increase monotonically with *x*. The lattice parameters show linear concentration dependences and well obey the Vegard's law of solid solutions. Our results are qualitatively in agreement with the previously reported results using polycrystalline samples obtained by HP and HT technique[31], and also agree well with the theoretically predicted lattice parameters of the hypothetical compound $Fe_3Sn_2S_2$ of shorter *a* (5.343 Å) and longer *c* (13.479 Å)[39]. It should be noted that the variation of the lattice parameters of our single crystals is rather steeper than that of the polycrystalline samples. The difference in the Fe-concentration dependences between our results and previous ones using polycrystalline samples are more clearly found in the magnetic properties described in the following subsection.

The increase of the ratio of *c* to *a* against *x* indicates an enhancement of the trigonal distortion by the Fe-substitution. Indeed, corresponding to the opposite behavior of lattice parameters against *x*, the interlayer *d*(*T*-Sn1) bond length increases while *d*(*T*-Sn2) = *d*(*T*-*T*) = *a*/2, within the kagomé layers, shrink upon Fe-substitution. The bond lengths between *T* and Sn atoms at the two different sites Sn1 and Sn2 which are almost equal *d*(*T*-Sn1) ≃ *d*(*T*-Sn2) for *x* = 0, slightly split to *d*(*T*-Sn1) > *d*(*T*-Sn2) by the Fe-substitution as a manifestation of the enhancement of the trigonal distortion. It should be noted that the increase of c/a, equivalently the trigonal distortion, by the Fe-substitution is much smaller than that caused by the In-substitution[4,22,25]. The DFT calculations predicted the energy gap opening and the significant enhancement of the trigonal distortion in the In-substituted systems caused by the In-Sn ordering: the In atoms occupy only the interlayer Sn1-site[19]. Indeed, the partial ordering of the In-Sn

atoms, the prefer substitution of In to the Sn1-site, was found by a recent neutron diffraction experiment[40]. On the contrary, a weak structure distortion was predicted in the Fe-substituted systems[39]. In both systems, the main effect of the substitution is a reduction of electron number: one electron in 3*d*- and 5*p*-orbitals are reduced in the Fe- and In-substituted systems, respectively. The enhancement of the trigonal distortion in the In-substituted $Co_3Sn_{2-y}In_yS_2$ was explained by the anisotropy of the In 5*p*-orbitals in DFT model calculations[22], which can also explain the smallness of the enhancement of trigonal distortion in $Co_{3-x}Fe_xSn_2S_2$.

3.3. Magnetic Properties

The temperature dependences of the magnetic susceptibility, M/H, of $Co_{3-x}Fe_xSn_2S_2$ single crystals with H // c are shown in Fig. 5, where M is the magnetization and H is the applied magnetic field. Arrott plot of the magnetic isotherms of $Co_3Sn_2S_2$ (not shown) indicates the precise Curie temperature T_C = 174 K (± 0.5 K) and the spontaneous moment in the easy c-axis at 2 K is $\mu_s \sim 0.3\ \mu_B$/Co, which are in agreement with the previously reported ones[23,25]. The ferromagnetic order is suppressed upon Fe-substitution but is not collapsed until the solubility limit. The inset of Fig. 5 shows the magnetic phase diagram of $Co_{3-x}Fe_xSn_2S_2$ obtained by using our single crystals. The critical concentration of the ferromagnetic order is roughly estimated to be $x_c \sim 0.8$ by extrapolating the T_C-x relation below the solubility limit x = 0.53 to T_C = 0. It is lower than the reported value, x = 1.5, estimated using polycrystalline samples obtained by HP and HT technique with the Fe-concentration exceeding the solubility limit at ambient pressure[31]. This discrepancy can be explained by the overestimation of the critical concentration due to a probable reduction of the actual Fe concentration in polycrystalline samples above the solubility limit, as well as observed in our single crystals for $x_{nom} > 0.5$.

According to the electronic band calculation, $Co_3Sn_2S_2$ has a pseudo-gap just below the Fermi level and its ferromagnetism attributes to a lift of the spin degeneracy of the half-filled band just above the pseudo-gap[13]. Hence, it is expected that reduction of the electron number, due to the element substitution for instance, causes a suppression of the ferromagnetism. Furthermore, simultaneous

emergence of semiconducting gap opening and ferromagnetic-nonmagnetic quantum phase transition is also expected. To verify the significance of the electron number to the magnetic order, we compare the variations of Curie temperature in the two solid solution systems $Co_{3-x}Fe_xSn_2S_2$ and $Co_3Sn_{2-y}In_yS_2$[25] against the substituted concentrations x and y, where x and y in the two systems correspond to the reduced electron number per one formula unit. The variations of Curie temperature are almost identical in both Fe- and In-substituted systems, indicating that the electron number, regardless the substituted elements, is the most dominant parameter to control the magnetism in the half-metallic ferromagnet $Co_3Sn_2S_2$. Other effects by the substitutions should be less relevant to the magnetism. For instance, it is well known that itinerant electron magnetism is enhanced in general as the unit cell volume, V, increases, whereas the opposite behavior of T_c against V was observed, T_C is suppressed with the increasing of V by Fe-substitution as shown in the insets of Figs. 4 and 5. Moreover, the *c/a* ratios in the Fe- and In-substituted systems are quite different as shown in the inset of Fig. 6, nevertheless the magnetic phase diagram in both systems are almost identical as mentioned above. The importance of the electron count on the magnetism of the shandite compounds based on our results suggests the validity of the DFT predictions of half metallic state with higher magnetic moments of the hypothetical shandite with lower electron count, $Fe_3Sn_2S_2$, as the Fermi level is shifted to higher DOS maxima[39]. The suppression of the ferromagnetic order of $Co_3Sn_2S_2$ was also observed in the Ni-substituted system[29], where the one *d*-electron per formula unit increases on the contrary to the Fe- and In-substituted systems, indicating that $Co_3Sn_2S_2$, where the band with the majority-spin channel is half filled, has the highest Curie temperature. It suggests that increased electrons in $Co_3Sn_2S_2$, caused by the Ni-substitution for instance, fill the minority spin band rather than the majority spin band.

4. Conclusion

Single crystals of the shandite solid solution $Co_{3-x}Fe_xSn_2S_2$ ($0 < x \leq 0.53$) of stacked metallic layers, consist of Co/Fe kagomé network permeated by Sn triangular lattice, have been successfully grown out of Sn self flux. Pb flux is also available for synthesizing the single crystals with only lower Fe

concentration. The grown crystals were characterized by means of the WDX, Laue X-ray photography, PXRD and magnetization measurements. The solubility limit, structural and magnetic properties observed in our single crystals are qualitatively in good agreement with the reported results using polycrystalline samples. The Rietvelt analyses of the PXRD data exhibits a much smaller enhancement of the trigonal distortion in the Fe-substituted crystals than that in the In-substituted ones. The suppression of the ferromagnetic order caused by the Fe-substitution was observed, as well as by the In-substitution. The magnetic phase diagram of $Co_{3-x}Fe_xSn_2S_2$ is obtained and the critical Fe concentration $x_c \sim 0.8$ was estimated by extrapolating the T_C-x relation below the solubility limit to $T_C = 0$. Almost identical magnetic phase diagrams in both Fe- and In-substituted systems clearly indicate the significance of the electron number to the ferromagnetism in $Co_3Sn_2S_2$.

AUTHOR INFORMATION

Corresponding Author

* E-mail: kassem.ahmed.82s@st.kyoto-u.ac.jp

Permanent Addresses

† Department of Physics, Assiut University, Assiut 71515, Egypt

ACKNOWLEDGMENT

M. A. K. would like to thank the Egyptian Ministry of Higher Education for financial support during his study in Japan.

Figure Captions:

Figure 1. (a) Crystal structure of the shandite-phase $Co_3Sn_2S_2$ showing the stacking metallic layers along the *c* direction in ABC fashion. The polyhedra represent Sn_4S_2 around Co-sites. (b) One metallic layer in *ab* plane consisting of corner-sharing triangles of Co atoms arranged in the 2D kagomé lattice and triangular lattice of Sn atoms. These structures were drawn using the VESTA software[24] .

Figure 2. (a) Images of grown single crystals of $Co_{3-x}Fe_xSn_2S_2$ out of Sn flux on a mm scale, (b) Experimental back Laue image taken from the large flat plane of the sheet-shaper single crystal shown in the inset and (c) the corresponding calculated Laue image of the (0 0 1) plane.

Figure 3. (Color online) Powder X-ray diffraction patterns of $Co_{3-x}Fe_xSn_2S_2$ single crystals with representative *x* measured at room temperature. Observed, refined patterns using the Rietveld method and differences between them are shown in open circles, red solid lines and black solid lines, respectively. Bragg reflection angles of $Co_3Sn_2S_2$ phase are indicted as vertical bars in the lowest panel. The reliability *R*-factors, as well as the goodness-fit-indicator *S*, for each pattern are indicated. Inset shows the absence of the by-products peaks in a normalized patterns of well polished crystals of $Co_3Sn_2S_2$ (green circles) compared to the patterns used in the Rietveld analysis shown in the main figure (blue circles).

Figure 4. Fe concentration dependence of the lattice parameters *a* and *c*. Inset shows the *c/a* ratio (on left) and unit cell volume (on right) against *x* of $Co_{3-x}Fe_xSn_2S_2$ single crystals.

Figure 5. (a) Temperature dependences of *M*/*H* of $Co_{3-x}Fe_xSn_2S_2$ ($0 \leq x \leq 0.5$) measured at $H = 0.1$ T applied along *c* direction. Inset shows the obtained magnetic phase diagram of $Co_{3-x}Fe_xSn_2S_2$, solid and extrapolated dashed lines are for eye guidance.

Figure 6. Fe and In concentration dependences of Curie temperature in $Co_{3-x}Fe_xSn_2S_2$ and $Co_3Sn_{2-y}In_yS_2$. Inset shows the *x* and *y* dependences of *c/a* ratio in both solid state solutions.

5. REFERENCES

(1) Fredrick, S. J.; Prieto, A. L. *J. Am. Chem. Soc.* **2013**, *135* (49), 18256–18259.

(2) Wagner, S.; Shay, J. L.; Migliorato, P.; Kasper, H. M. *Appl. Phys. Lett.* **1974**, *25* (8), 434–435.

(3) Chen, B.; Uher, C.; Iordanidis, L.; Kanatzidis, M. G. *Chem. Mater.* **1997**, *9* (7), 1655–1658.

(4) Corps, J.; Vaqueiro, P.; Aziz, A.; Grau-Crespo, R.; Kockelmann, W.; Jumas, J.-C.; Powell, A. V. *Chem. Mater.* **2015**, *27* (11), 3946–3956.

(5) Ramirez, A. P.; Cava, R. J.; Krajewski, J. *Nature* **1997**, *386* (13), 156–159.

(6) Ando, K.; Nishihara, Y.; Okuda, T.; Tsushima, T. *J. Appl. Phys.* **1979**, *50* (B3), 1917.

(7) Scholtz, D. L. *Trans. Geol. Soc. S. Africa* **1937**, *39*, 81–210.

(8) Ramdohr, P. *Sitz. Berl. Akad. Wiss. Math.-Nat. Kl. VI* **1949**, *1*.

(9) Weihrich, R.; Matar, S. F.; Eyert, V.; Rau, F.; Zabel, M.; Andratschke, M.; Anusca, I.; Bernert, T. *Prog. Solid State Chem.* **2007**, *35* (2-4 SPEC. ISS.), 309–327.

(10) Weihrich, R.; Anusca, I. *Z. Anorg. Allg. Chem.* **2006**, *632* (2), 335–342.

(11) Weihrich, R.; Anusca, I.; Zabel, M. *Z. Anorg. Allg. Chem.* **2005**, *631* (8), 1463–1470.

(12) Weihrich, R.; Anusca, I.; Zabel, M. *Z. Anorg. Allg. Chem.* **2004**, *630* (11), 1767–1767.

(13) Weihrich, R.; Anusca, I. *Z. Anorg. Allg. Chem.* **2006**, *632* (8-9), 1531–1537.

(14) Zabel, M.; Wandinger, S.; Range, K.; Prof, S.; Regensburg, D. *Z. Naturforsch* **1979**, *34B*, 238–241.

(15) Natarajan, S.; Rao, G. V. S.; Baskaran, R.; Radhakrishnan, T. S. *J. Less Common Met.* **1988**, *138* (2), 215–224.

(16) Zabel, M.; Wandinger, S. and Range, K. *Rev. Chim. Miner.* **1983**, *20*, 698.

(17) Michelet, A.; Collin, G.; Gorochov, O. *J. Less Common Met.* **1984**, *97*, 73–78.

(18) Sakamoto, T.; Wakeshima, M.; Hinatsu, Y. *J. Phys. Condens. Matter* **2006**, *18* (17), 4417–4426.

(19) Rothballer, J.; Bachhuber, F.; Pielnhofer, F.; Schappacher, F. M.; Pöttgen, R.; Weihrich, R. *Eur. J. Inorg. Chem.* **2013**, *2* (2), 248–255.

(20) Corps, J.; Vaqueiro, P.; Powell, A. V. *J. Mater. Chem. A* **2013**, *1* (22), 6553.

(21) Fujioka, M.; Shibuya, T.; Nakai, J.; Yoshiyasu, K.; Sakai, Y.; Takano, Y.; Kamihara, Y.; Matoba, M. *Solid State Commun.* **2014**, *199*, 56–60.

(22) Pielnhofer, F.; Rothballer, J.; Peter, P.; Yan, W.; Schappacher, F. M.; Pöttgen, R.; Weihrich, R. *Z. Anorg. Allg. Chem.* **2014**, *640* (2), 286–294.

(23) Schnelle, W.; Leithe-Jasper, a.; Rosner, H.; Schappacher, F. M.; Pöttgen, R.; Pielnhofer, F.; Weihrich, R. *Phys. Rev. B* **2013**, *88* (14), 1–8.

(24) Momma, K.; Izumi, F. *J. Appl. Crystallogr.* **2008**, *41* (3), 653–658.

(25) Kassem, M. A.; Tabata, Y.; Waki, T.; Nakamura, H. *J. Cryst. Growth* **2015**, *426*, 208–213.

(26) Holder, M.; Dedkov, Y.; Kade, a.; Rosner, H.; Schnelle, W.; Leithe-Jasper, a.; Weihrich, R.; Molodtsov, S. *Phys. Rev. B* **2009**, *79* (20), 1–7.

(27) Umetani, A.; Nagoshi, E.; Kubodera, T.; Matoba, M. *Phys. B Condens. Matter* **2008**, *403* (5-9), 1356–1358.

(28) Sakai, Y.; Kamihara, Y.; Matoba, M. *Phys. Status Solidi* **2013**, *10* (7-8), 1130–1131.

(29) Weihrich, R.; Yan, W.; Rothballer, J.; Peter, P.; Rommel, S. M.; Haumann, S.; Winter, F.; Schwickert, C.; Poettgen, R. *Dalt. Trans.* **2015**, *44*, 15855–15864.

(30) Kubodera, T.; Okabe, H.; Kamihara, Y.; Matoba, M. *Phys. B Condens. Matter* **2006**, *378-380*, 1142–1143.

(31) Sakai, Y.; Tanakadate, R.; Matoba, M.; Yamada, I.; Nishiyama, N. *J. Phys. Soc. Jpn.* **2015**, *84*, 044705.

(32) Fisk, Z.; Remeika, J. P. In *Handbook on the Physics and Chemistry of Rare Earths. vol. 12*; Gschneidner Jr, K.A. and Eyring, L., Ed.; Elsevier: Amsterdam, 1989; pp 53–70.

(33) Canfield, Paul C. and Fisk, Z. *Philos. Mag. B* **1992**, *65* (6), 1117–1123.

(34) Canfield, P. C.; Fisher, I. R. *J. Cryst. Growth* **2001**, *225* (2-4), 155–161.

(35) Kanatzidis, M. G.; Pöttgen, R.; Jeitschko, W. *Angew. Chemie - Int. Ed.* **2005**, *44* (43), 6996–7023.

(36) Canfield, P. C. In *Properties and Applications of Complex Intermetallics*; E. Belin-Ferré, Ed.; World Scientific: Singapore, 2010; pp 93–111.

(37) Lin, X.; Bud'ko, S. L.; Canfield, P. C. *Philos. Mag.* **2012**, *92* (19-21), 2436–2447.

(38) Bruker AXS (2008): TOPAS V4: General profile and structure analysis software for powder diffraction data. - User's Manual, Bruker AXS, Karlsruhe, Germany.

(39) Pielnhofer, F.; Tragl, A. S.; Rothballer, J.; Weihrich, R. *Z. Naturforsch.* **2014**, *69B*, 55–61.

(40) Rothballer, J.; Bachhuber, F.; Rommel, S. M.; Söhnel, T.; Weihrich, R. *RSC Adv.* **2014**, *4* (79), 42183–42189.

Tables

Table 1: The used flux; chemical configuration and actual Fe concentration based on WDX measurements.

Nominal *x*	Flux	Chemical configuration	Actual *x*
0.00	Sn	$Co_3Sn_{2.09}S_{2.06}$	0.00
0.10	Sn	$Co_{2.86}Fe_{0.14}Sn_{2.01}S_{1.83}$	0.14
0.25	Sn	$Co_{2.61}Fe_{0.39}Sn_{1.96}S_{1.81}$	0.39
0.50	Sn	$Co_{2.51}Fe_{0.49}Sn_2S_{1.84}$	0.49
0.60	Sn	$Co_{2.51}Fe_{0.49}Sn_{2.06}S_{1.99}$	0.49
0.70	Sn	$Co_{2.47}Fe_{0.53}Sn_{2.05}S_{1.94}$	0.53
0.75	Pb	$Co_{2.68}Fe_{0.32}Sn_{1.96}S_{1.83}$	0.32
1.00	Pb	$Co_{2.51}Fe_{0.49}Sn_2S_{1.84}$	0.29

Table 2: Lattice parameters, atomic position parameter of sulfur, *z*, and atomic bond lengths of $Co_{3-x}Fe_xSn_2S_2$ refined by the Rietveld analysis of PXRD patterns at room temperature using the TOPAS software. The shandite phase with space group $R\bar{3}m$ and atomic positions of Co/Fe at 9*e*(½,0,0), Sn1 at 3*b*(0,0, ½), Sn2 at 3*a*(0,0,0) and S at 6*c*(0,0,*z*) is assumed (see text).

x	*a* /Å	*C* /Å	*z*	d(*T*-Sn1) /Å	d(*T*-Sn2/*T*) /Å	d(*T*-S) Å
0.00	5.3683(2)	13.1783(5)	0.2161(3)	2.68807	2.68417	2.188(3)
0.14	5.3681(4)	13.18758(9)	0.2134(5)	2.68958	2.68439	2.215(4)
0.29	5.3672(4)	13.1947(9)	0.2155(3)	2.69012	2.68361	2.195(3)
0.32	5.3671(2)	13.1950(5)	0.2142(2)	2.69016	2.68359	2.206(2)
0.39	5.3670(7)	13.199(2)	0.2167(3)	2.69074	2.68353	2.184(2)
0.49	5.3667(3)	13.2065(6)	0.2161(3)	2.69169	2.68341	2.190(3)
0.53	5.3665(6)	13.206(2)	0.2170(3)	2.69165	2.6833	2.182(3)

Figure 1

Click here to download high resolution image

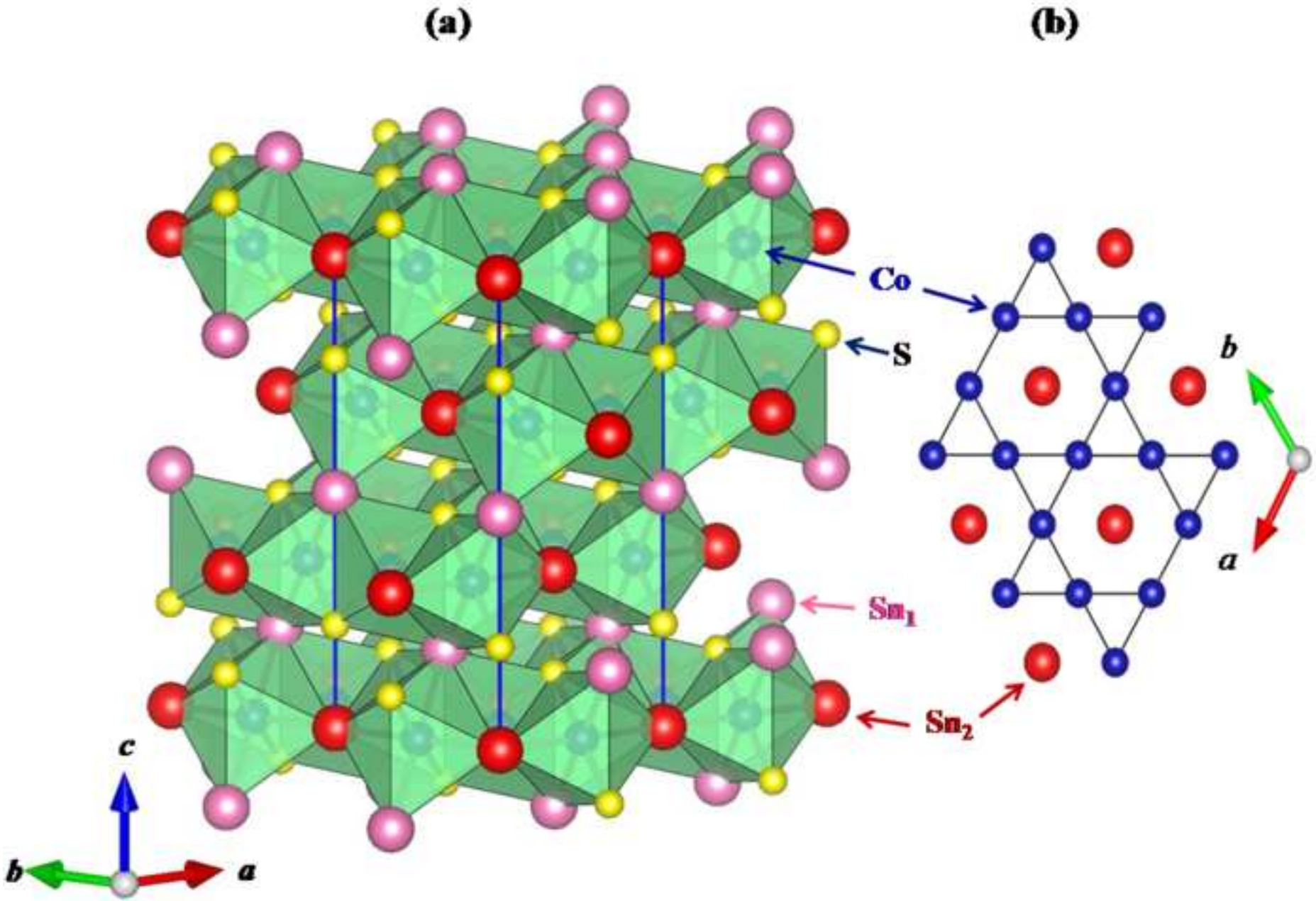

Figure 2

Click here to download high resolution image

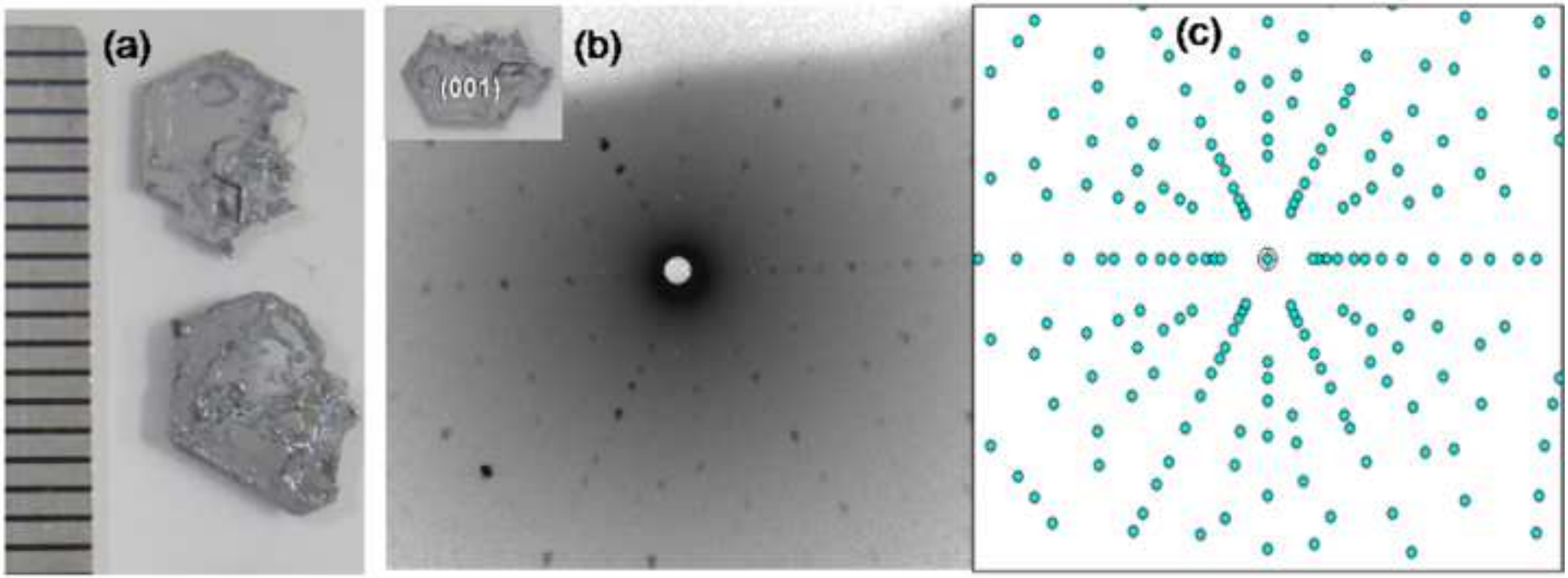

Figure 3

Click here to download Figure(s): Figure 3.eps

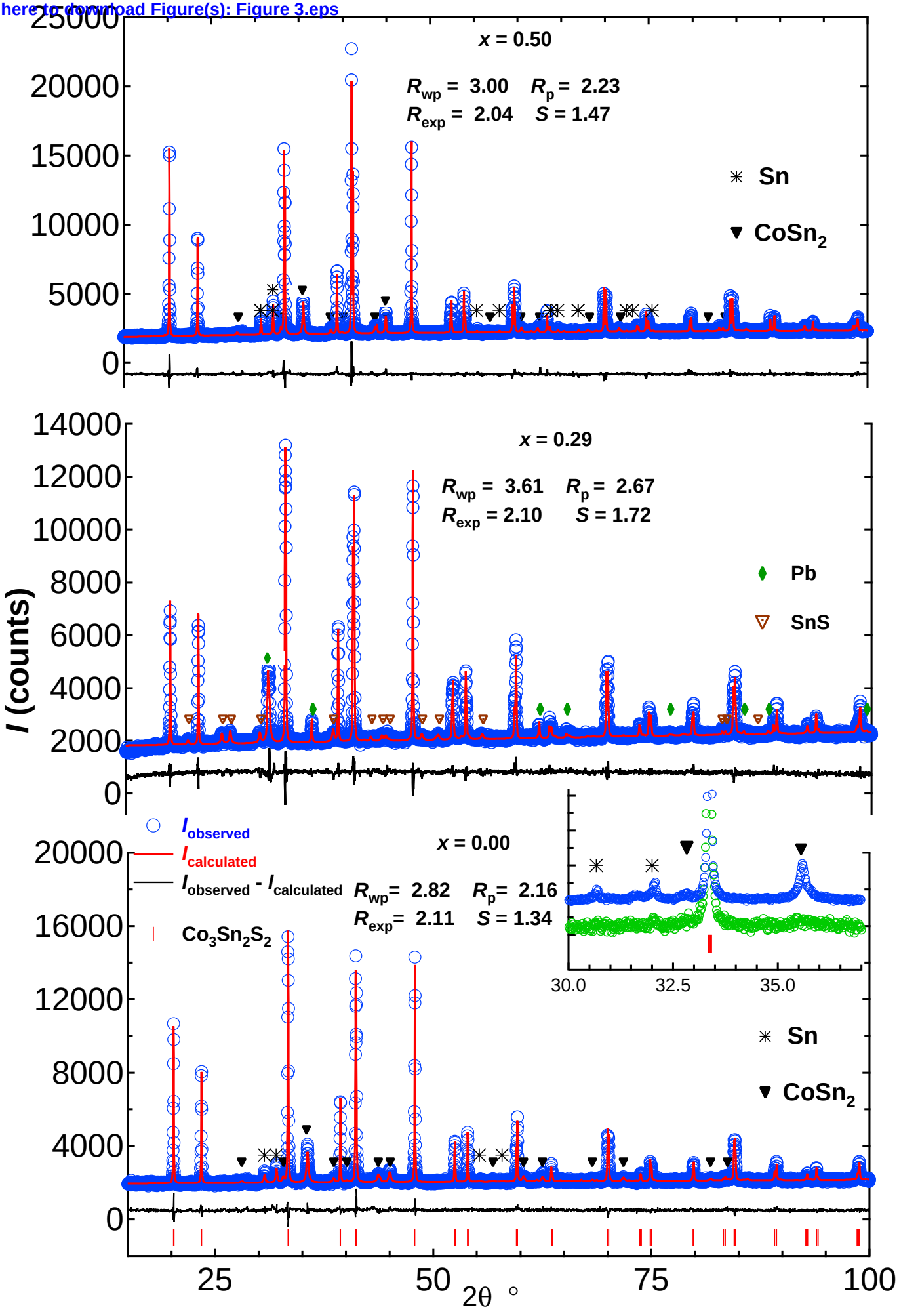

Figure 4

Click here to download Figure(s): Figure 4.eps

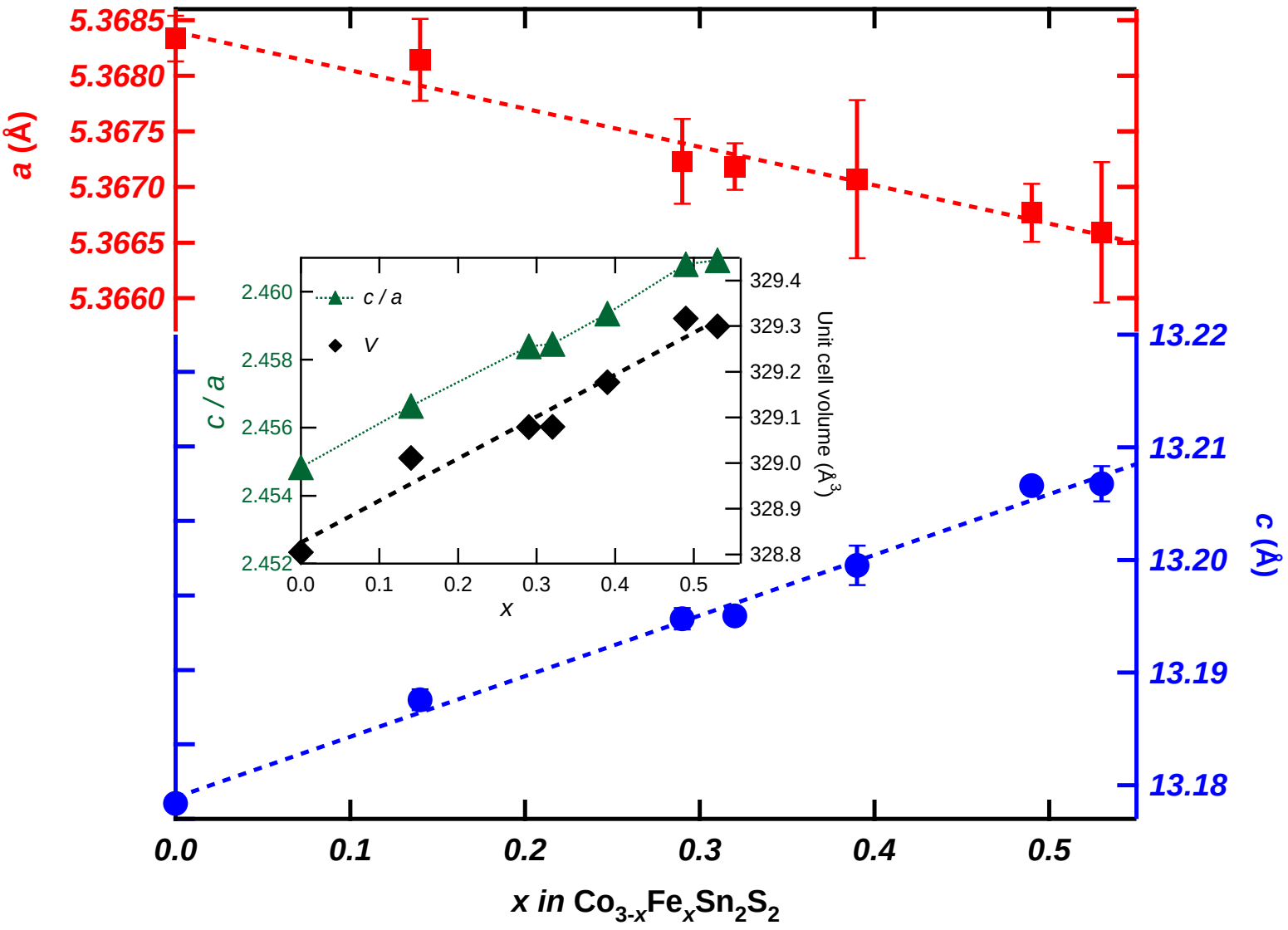

Figure 5

Click here to download Figure(s): Figure 5.eps

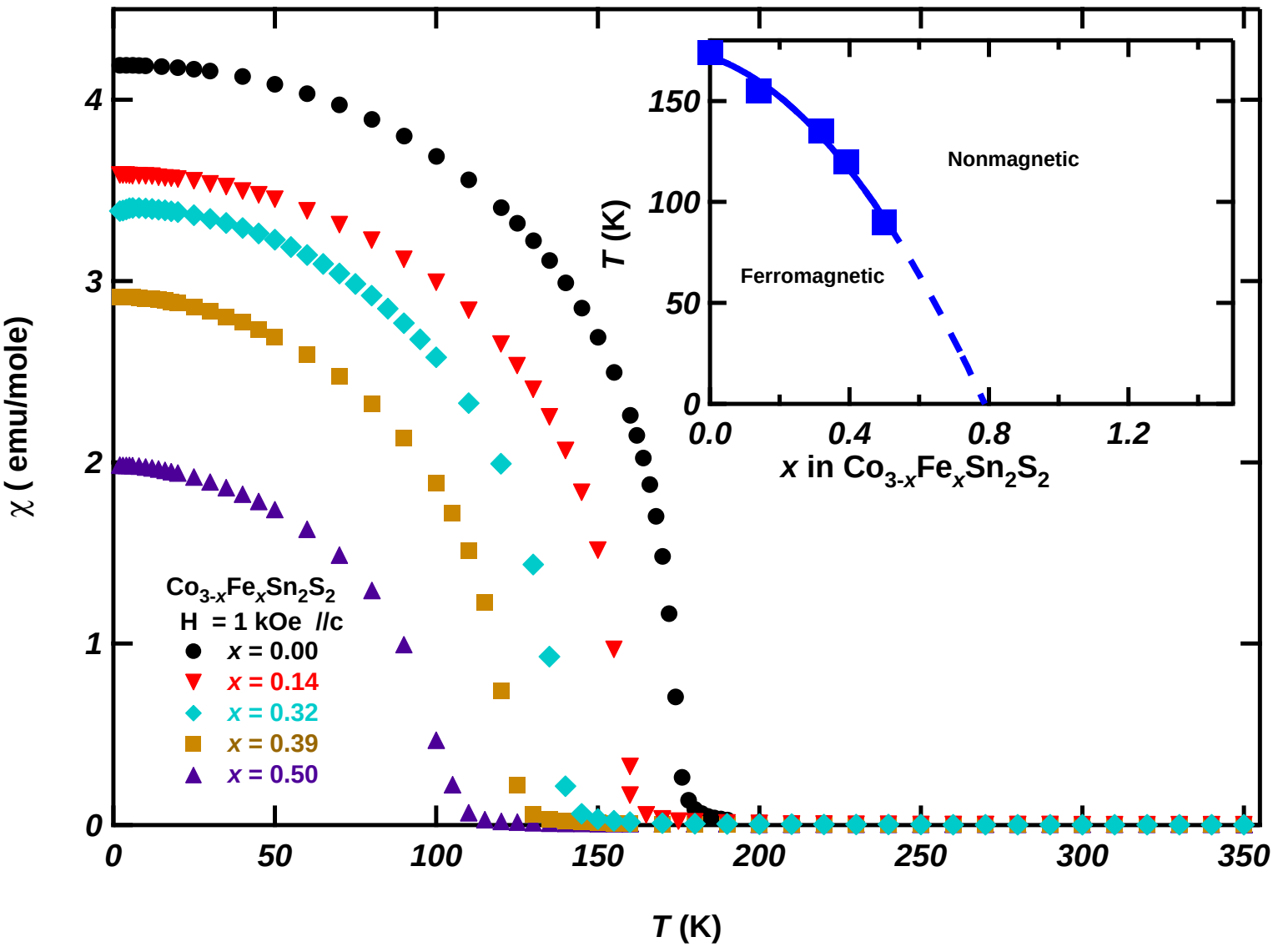

Figure 6

Click here to download Figure(s): Figure 6.eps

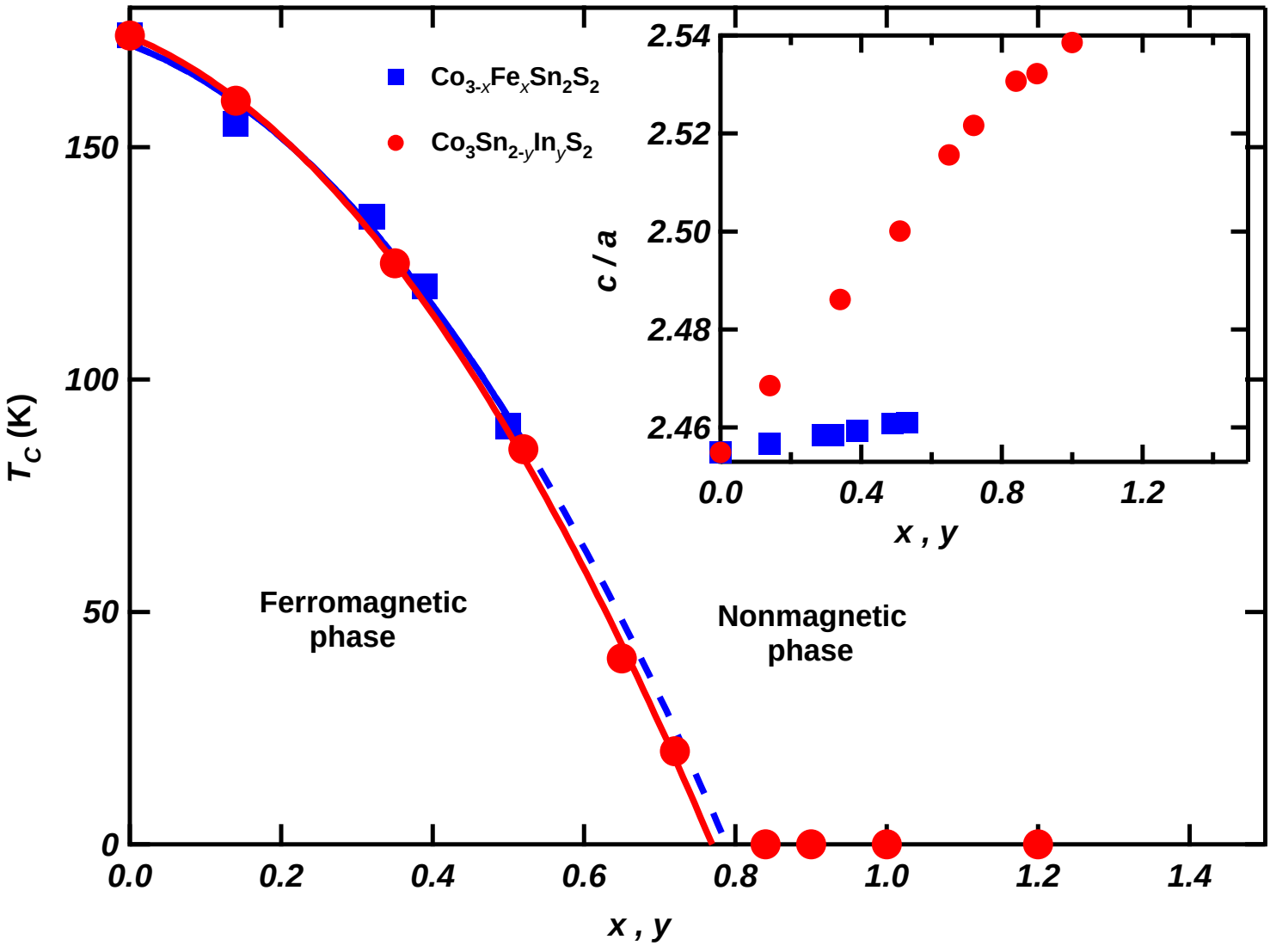

*Graphical Abstract

Click here to download high resolution image

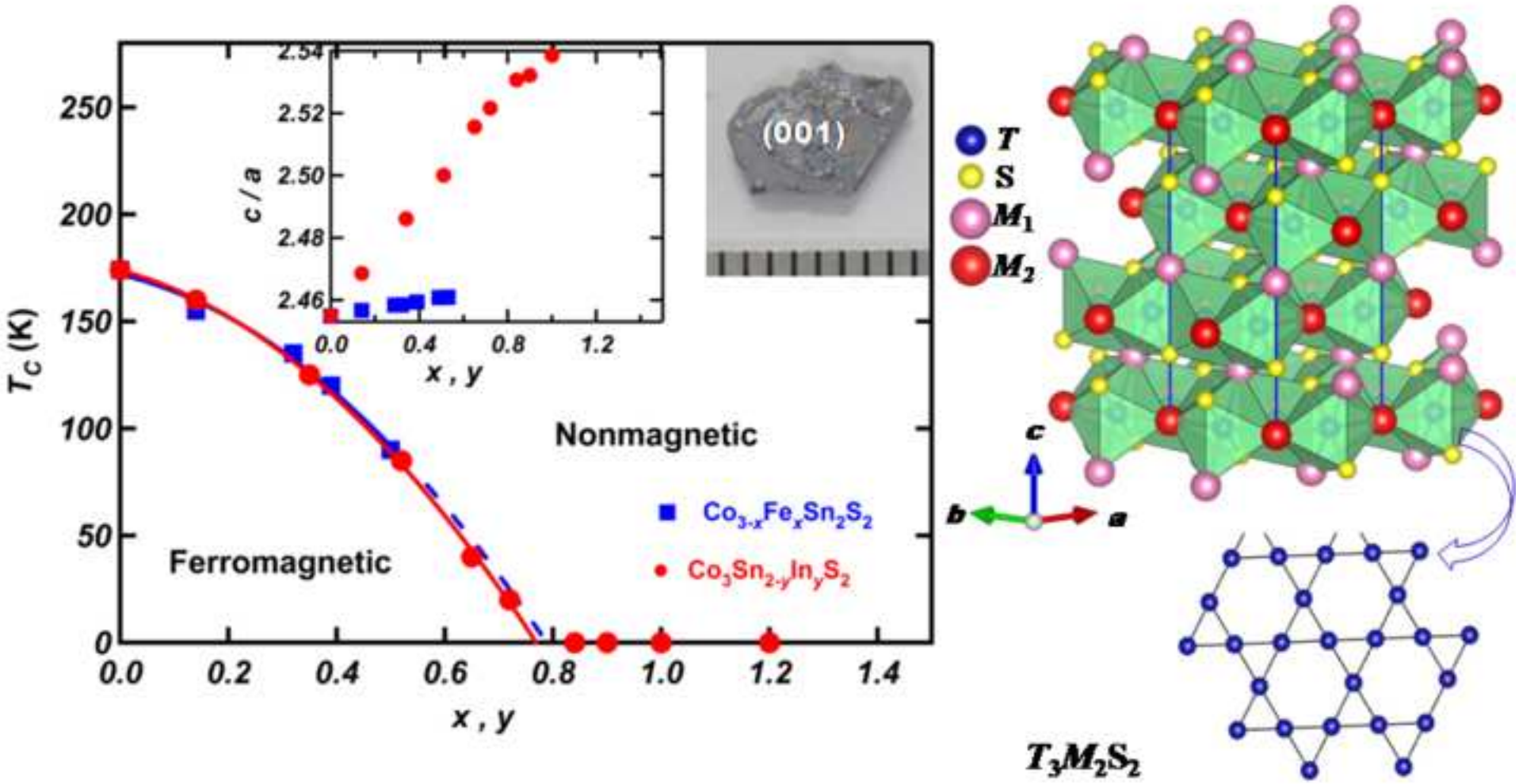

*Graphical Abstract Legend (TOC Figure)

Click here to download Graphical Abstract Legend (TOC Figure): Graphical Abstract Legand.docx

Graphical Abstract Legand of

Ms. No.: JSSC-15-1071:Structure and Magnetic Properties of Flux Grown Single Crystals of $Co_{3-x}Fe_xSn_2S_2$ Shandites.

Mohamed A. Kassem[*,†] , *Yoshikazu Tabata, Takeshi Waki, Hiroyuki Nakamura.*

Graphical Abstract Legend :

Magnetic phase diagrams of $Co_{3-x}Fe_xSn_2S_2$ and $Co_3Sn_{2-y}In_yS_2$ and general crystal structure of $T_3M_2S_2$ (T = Co, Fe and M = Sn, In) Shandites. Inset on left shows the x and y dependences of c/a ratio, respectively, while inset on right shows an image of a single crystal of $Co_{3-x}Fe_xSn_2S_2$ grown out of Sn flux on a mm scale.

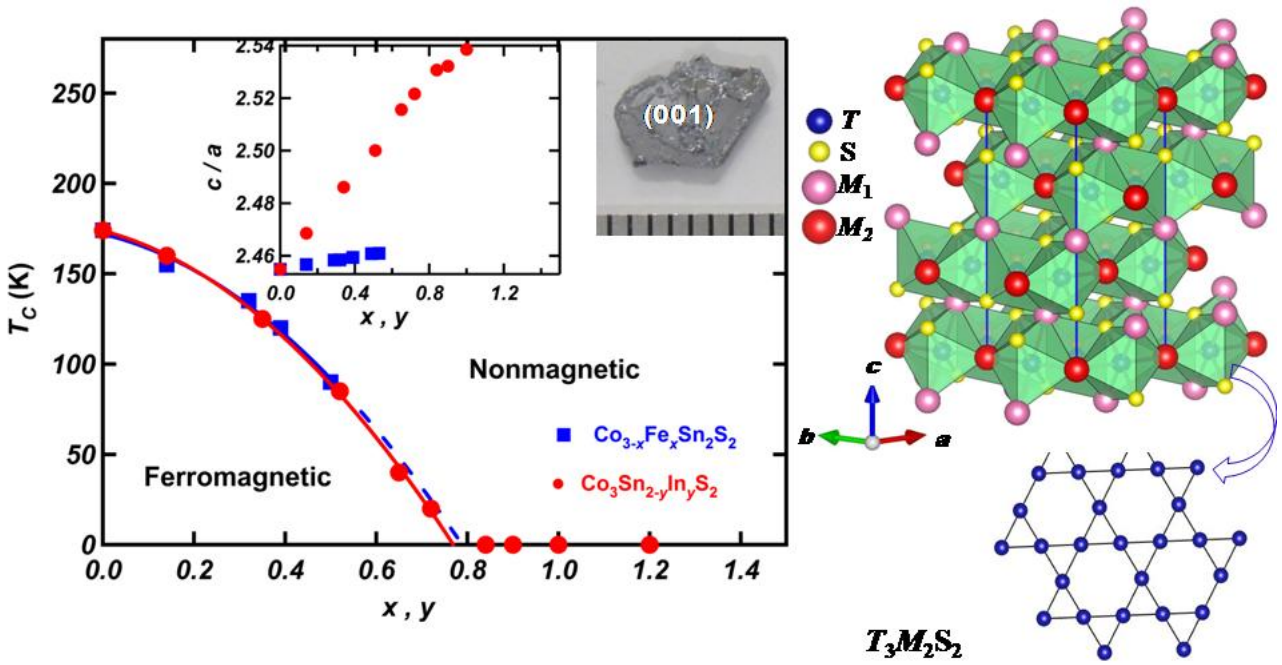

Highlights

- Successful growth of $Co_{3-x}Fe_xSn_2S_2$ crystals out of self Sn flux is reported.
- The solubility is limited to $x = 0.53$ as indicated by WDX spectroscopy.
- Unlike In-substitution, Fe results in much smaller crystal structure distortions.
- The obtained magnetic phase diagram indicates a magnetic transition at x_c=0.8.
- Our results indicate that the electron count mainly affects on magnetism of $Co_3Sn_2S_2$.